

Cross-sectional atomic force microscopy of ZnMgSSe- and BeMgZnSe-based laser diodes

A. V. Ankudinov,^{a)} A. N. Titkov, T. V. Shubina, S. V. Ivanov, and P. S. Kop'ev
Ioffe Physico-Technical Institute, St. Petersburg 194021, Russia

H.-J. Lugauer, G. Reuscher, M. Keim, A. Waag, and G. Landwehr
Physikalisches Institut der Universität Würzburg, Am Hubland, D-97074 Würzburg, Germany

(Received 4 June 1999; accepted for publication 31 August 1999)

Atomic force microscopy (AFM) of cleaved facets of ZnSe-based lasers with various active region designs is reported. Different AFM probe friction on the materials forming the laser structures are exploited for imaging their basic layers. Unlike ZnMgSSe-based lasers, the cleaved surface of cladding layers in BeMgZnSe-based structures is atomically flat, which is attributed to hardening of the II-VI materials by Be incorporation. Nanometer-high steps and undulations are observed at the laser heterointerfaces on cleaved facets. The shape and height of such topographic singularities located in the vicinity of a (Zn,Cd)Se quantum well active region depend on the strain distribution in the laser waveguide. © 1999 American Institute of Physics. [S0003-6951(99)05343-7]

ZnSe-based materials are still considered as the main candidates for fabrication of a commercial injection laser in the green spectral range.¹ The successful development of these devices it is necessary to increase an activation energy of the extended defects formation in II-VI materials. A promising approach to solve these problems is to employ Be-containing compounds that were shown to increase significantly the covalent component of the bond, thus "hardening" the material.^{2,3} Simultaneously, the durability of the II-VI lasers can be improved due to an efficient strain redistribution in the active region by the incorporation of an alternately strained superlattice (SL) waveguide lattice matched to a GaAs substrate.⁴

Cross-sectional characterization of cleaved semiconductor heterostructures by conventional techniques, like scanning electron microscopy (SEM) and transmission electron microscopy (TEM), provides valuable information on the thickness of constituent layers, interface roughness, and extended defect distribution. However, the cleavage surface relief itself can give direct insight into the mechanical properties of the heterolayers. A high stress developed at the tip of a moving cleavage crack may serve as an effective probe of a yield stress, and hence, hardness of strained layers, leading to either plastic or elastic deformation of the layers. As a result, abrupt or gradual topographic singularities can arise on the cleavage surface.

Indeed, a few atomic-scale studies of cleavages of semiconductor heterostructures were performed, revealing, for instance, nanometer-high topographic singularities along the interfaces.⁵⁻⁷ A cross-sectional atomic force microscopy (AFM) study of the ZnSe-based heterostructure found that the shape of the singularity at the II-VI/GaAs interface could change from ridgelike to steplike after incorporation at this interface of a strain-compensated SL.⁵ Bratina, Vanzetti, and Franciosi⁶ found that the height of the singularities at a strained quantum well (QW) layer in the ZnSe-based hetero-

structures depends on the lattice mismatch of the QW. They proposed that the surface relief could form due to the cleavage crack deviation at the interface between two materials with different fracture toughness by gliding of misfit dislocations. The lateral force microscopy (LFM) mode of the AFM was applied to distinguish directly the different semiconductor layers in a heterostructure.

In this letter, we report the cross-sectional AFM and LFM studies of ZnMgSSe- and BeMgZnSe-based laser heterostructures of different designs.^{2,4,8} To reveal the effect of Be incorporation, two lasers of a conventional type are investigated. These S- or Be-lasers involve a bulk 0.2 μm ZnS_{0.11}Se_{0.89} (or Be_{0.03}Zn_{0.97}Se) waveguide centered with a 10 nm Zn_{0.75}Cd_{0.25}Se QW (or 4 nm Zn_{0.63}Cd_{0.37}Se QW), surrounded by 1- μm -thick wide-band-gap *n*- and *p*-ZnMgSSe (or BeMgZnSe) cladding layers. Besides, two additional Be-containing structures with a (1 nm Be_{0.05}Zn_{0.95}Se/1.5 nm ZnSe)₈₂ SL waveguide. The first structure (SL Be-laser) has the conventional QW, while in the second one (FM SL Be-laser) such a QW is exchanged by a fractional monolayer (FM) 2.8 ML-CdSe/10 nm-ZnSe nanostructure.

The freshly cleaved samples were studied in air by AFM (P-4 SPM, NT-MDT) operating in contact mode, with a net constant force of about 80 nN. Commercial Si₃N₄ triangular cantilevers (Olympus, Japan) were used with a normal elastic constant of 0.68 N/m and with radius of curvature of the probe tip of less than 20 nm. To minimize cross talk between normal and lateral deflections of the cantilever, when taking the LFM images, a low scanning speed of $\sim 1 \mu\text{m/s}$ was employed.

Figure 1 presents cross-sectional AFM data and a schematic band-energy diagram for the S-laser. The AFM topography image of the laser cleavage in Fig. 1(a) reveals two surface singularities, running along the heterostructure interfaces: a 4-nm-high step and a 0.4-nm-deep ditch [see also the height profile in Fig. 1(b)]. The step is placed at the center of the waveguide area (W), while the ditch coincides with the II-VI/GaAs interface. Furthermore, we observe that the cleaved surface of the cladding layers is covered by tiny

^{a)}Electronic mail: alexander.ankudinov@pop.ioffe.rssi

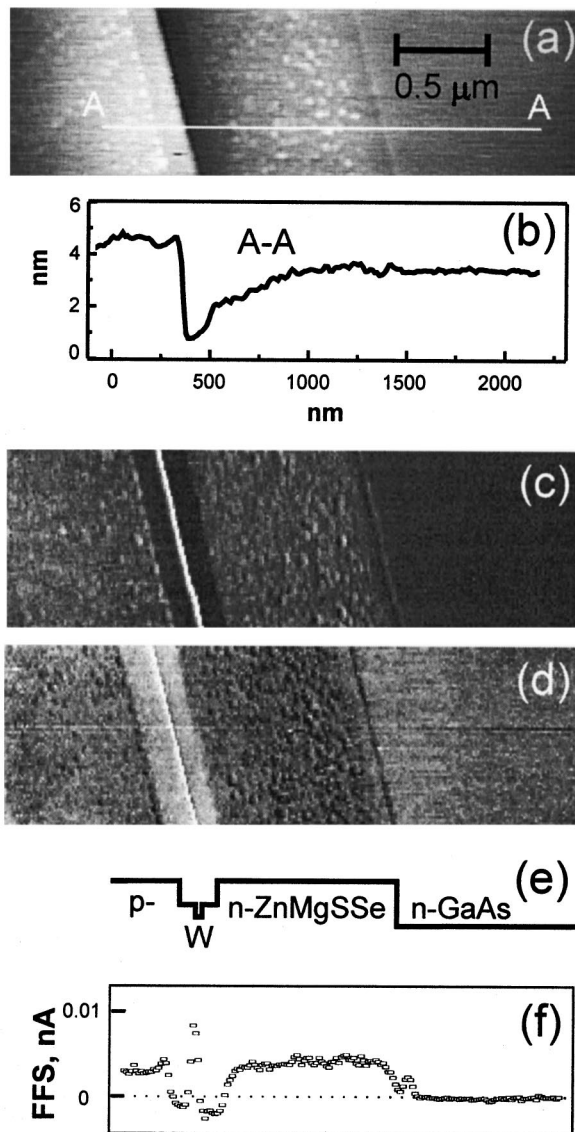


FIG. 1. (a) Cross-sectional AFM topography image of the S-containing structure, the full gray scale corresponds to a height variation of 7 nm; (b) height profile along the A–A line in (a); (c) and (d) LFM images obtained in left-to-right and right-to-left scanning directions from the same surface area; and (e) schematic laser diagram; (f) friction force cross profile of the structure, averaged along the interfaces.

hillocks with a height of a few nm and a surface density of around 10^{11} cm^{-2} .

In the LFM image from the same cleavage area [Fig. 1(c)], the signal of lower lateral deflection of the cantilever corresponds to the darker gray tones. The observed contrast arises mainly from the variation in friction between the tip and underlying layer surface, which is confirmed by the reversal of the contrast when the scanning direction is reversed, as shown in Fig. 1(d). The contrast of a bright line in the center of the waveguide is not reversed, since the line corresponds to a high step in the topography. At the sharp topographic features, the surface reaction force acts on the AFM tip at some angle to the mean normal to the surface, which leads to the lateral deflection of the cantilever, independent of the scanning direction.⁹ On the flat surface, the signal proportional to the friction force may be determined as a half difference between the lateral deflection signals mea-

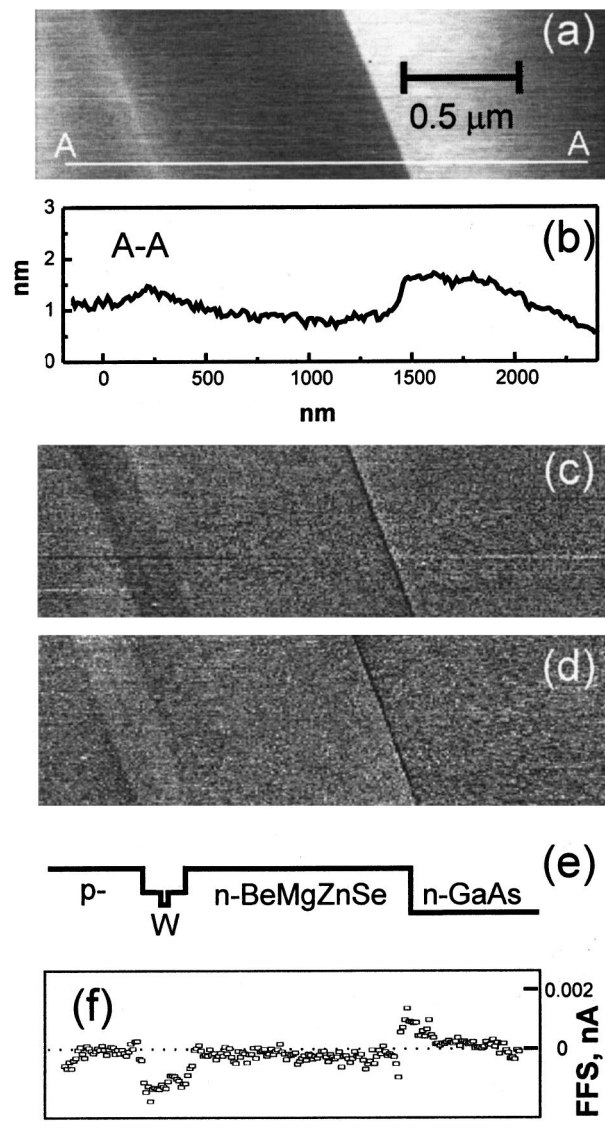


FIG. 2. (a) Cross-sectional AFM topography image of the Be-containing structure with a superlattice waveguide and a fractional monolayer active region, the full gray scale corresponds to a height variation of 1.8 nm; (b) height profile along the A–A line in (a); (c) and (d) LFM images obtained in opposite scanning directions from the same surface area; (e) schematic laser diagram; and (f) friction force cross profile of the structure, averaged along the interfaces.

sured in the opposite scanning directions.⁹ The resulting friction force cross profile of the structure, averaged along the interfaces, is presented in Fig. 1(f). A sharp peak corresponding to the bright line in the LFM images is displayed as the step in the AFM topography. It cannot be directly attributed to an increasing friction at the high step, since it results also from the insufficient suppression of the cross talk between normal and lateral deflections. Thus, the highest and lowest frictions are observed on the claddings and the waveguide, respectively.

Cross-sectional AFM data on the FM SL Be-laser are given in Fig. 2. From the LFM images measured at the same cleavage area in opposite scanning directions [Figs. 2(c) and 2(d)] and from the corresponding plot of the friction force [Fig. 2(f)], the waveguide region is directly identified as the one with the lowest friction. In the topography image [Fig. 2(a)], the positions of a 0.5-nm-high step and a 0.2-nm-high

TABLE I. Shape and height of a surface singularity at the waveguide center on cleavages of ZnSe-based lasers vs active region parameters.

Parameters\samples	S-laser	Be-laser	SL Be-laser	FM SL Be-laser
QW thickness (nm)	10	4	4	1
Lattice mismatch in QW (% to GaAs)	1.7	2.3	2.3	7
Mean height of singularity (nm)	3	1.7	0.25	0.2
Shape of singularity	Step	Step	Ridge	Ridge

ridge [see also the height profile in Fig. 2(b)] correspond to the GaAs/II–VI interface and the center of the waveguide, respectively. In contrast to the S-laser, the cleavages of the cladding layers in this structure look atomically flat. Similar friction force behavior and surface morphology have been found for cleavages of the other Be-containing structures. However, the Be-laser with a bulk waveguide demonstrates a much higher step at the QW (1.7 nm) instead of the low 0.2 nm ridge (for a summary, see Table I).

Thus, analysis of our topography data permits us to underline two observations: (1) an inequality in the surface morphology of the cladding layers of the studied S- and Be-containing lasers and (2) a dependence of the shape and height of the singularity at the waveguide position on the active region design. The surface density of the hillocks on the cladding layers of the S laser [Fig. 1(a)] is too high to attribute the hillocks to as-grown defects. The hillocks' height is strongly influenced by the cleavage technique used, allowing them to be considered as traces of plastic rupture of the cladding layers. An inelastic deformation of the material, accompanying such rupture, implies arising and gliding dislocations in the vicinity of the tip of the moving cleavage crack. In contrast to the S laser, almost perfectly smooth facets of the Be-laser claddings [e.g., Fig. 2(a)] suggest only elastic deformation of the Be chalcogenides during cleavage, i.e., the bonds of Be-containing materials are stretched elastically to their limit and then break suddenly without plastic deformation. The possibility of such brittle fracture may indicate a "hardening" of the Be-containing layers in comparison with the S-containing ones.

Table I shows the relation between the height and shape of the singularity in the waveguide area and the design of the active region. Instead of the high and sharp step placed at the QW for both types of conventional lasers, the significantly lower and broader ridge-like structure for two others lasers with a superlattice waveguide is observed. We can associate this difference in the surface morphology with the strain distribution in the active region, which is explained as follows.

For both lasers of conventional type, a large compressive strain is accumulated by the ZnCdSe QWs, which are ~2% lattice mismatched. The appearance of the step at the QW position can be energetically favorable, if the release of strain energy due to the step formation exceeds the increase

in the free-surface energy of the cleavage. Indeed, the data in Table I indicate that the height of this step is approximately proportional to the product of the lattice mismatch and the QW thickness. As a possible way of step emergence, slipping of the QW material along the {111} planes during cleavage can be supposed. This process may be facilitated due to a decrease in the yield stress of the highly strained QW layer, like an ordinary glass may be "toughened" and become less brittle after heat treatment inducing compressive self-stresses in the material.¹⁰

For the two laser structures with the SL waveguide, the strain induced by the QW can be significantly redistributed over the alternately strained SL waveguide due to its higher elasticity as compared to the bulk one, resulting in the dramatic reduction of the maximal stress magnitude. This is reflected in the subnanometer expansion of the waveguide area over the cleavage surface, revealed as a ridge in the AFM image in Figs. 2(a) and 2(b). A similar mechanism of relief formation on the cleavage over the stressed layers due to the elastic relaxation of the surface was suggested by Chen *et al.*⁷

In conclusion, we have demonstrated that laser heterostructure cleaved facets can be studied efficiently by AFM and LFM. Contrary to SEM and TEM techniques, one can visualize the strain distribution across the structure as subnanometer-scale surface relief modulations at the structure cleavage plain. The influence of the material hardness on the cleavage surface morphology has been observed and discussed. Direct dependence of the height of the interface step on the strain energy accumulated in the QW region has been found.

The authors would like to thank A. K. Kryghanovsky for data processing. This work was supported in part by RFBR, the Program of the Ministry of Sciences of RF "Physics of Solid State Nanostructures," Volkswagen Stiftung, and the INTAS Grant No. 97-31907.

¹E. Kato, H. Noguchi, M. Nagai, H. Okuyama, S. Kijima, and A. Ishibashi, *Electron. Lett.* **34**, 282 (1998).

²A. Waag, F. Fischer, K. Schüll, T. Baron, H.-J. Lugauer, Th. Litz, U. Zehnder, W. Ossau, T. Gerhardt, M. Keim, G. Reuscher, and G. Landwehr, *Appl. Phys. Lett.* **70**, 280 (1997).

³C. Verie, *J. Electron. Mater.* **27**, 782 (1998).

⁴S. V. Ivanov, A. A. Toropov, S. V. Sorokin, T. V. Shubina, A. V. Lebedev, P. S. Kop'ev, Zh. I. Alferov, H.-J. Lugauer, G. Reuscher, M. Keim, F. Fischer, A. Waag, and G. Landwehr, *Appl. Phys. Lett.* **73**, 2104 (1998).

⁵I. Suemune and M. Hoshiyama, *Jpn. J. Appl. Phys., Part 1* **33**, 3748 (1994).

⁶G. Bratina, L. Vanzetti, and A. Franciosi, *Phys. Rev. B* **52**, R8625 (1995).

⁷H. Chen, R. M. Feenstra, R. S. Goldman, G. Silfvén, and G. Landgren, *Appl. Phys. Lett.* **72**, 1727 (1998).

⁸S. V. Ivanov, A. A. Toropov, S. V. Sorokin, T. V. Shubina, I. V. Sedova, A. A. Sitnikova, P. S. Kop'ev, Zh. I. Alferov, H.-J. Lugauer, G. Reuscher, M. Keim, F. Fischer, A. Waag, and G. Landwehr, *Appl. Phys. Lett.* **74**, 498 (1999).

⁹D. F. Ogletree, R. W. Carpick, and M. Slameron, *Rev. Sci. Instrum.* **67**, 3298 (1996).

¹⁰A. H. Cottrell, *The Mechanical Properties of Matter* (Wiley, New York, 1964), Chap. 11.